Parameter identification of a mechanical ductile damage using Artificial Neural Networks in sheet metal forming.

Fethi Abbassi, Touhami Belhadj, Sébastien Mistou, Ali Zghal

Parameter identification of a mechanical ductile damage using Artificial Neural Networks in sheet metal forming

Fethi Abbassi [a,*], Touhami Belhadj [a], Sébastien Mistou [b], Ali Zghal [a]

[a] URMSSDT-ESST Tunis, 5 Avenue Taha Hussein, BP, 56, Bâb Manara 1008, Tunisia
[b] Université de Toulouse, INP/ENIT, M2SP-LGP, 47 Avenue d'Azereix, 65016 Tarbes, France

Keywords:
Ductile damage
Identification
Artificial Neural Networks
Metal forming
Experimental mechanics
Numerical Simulation

A B S T R A C T

In this paper, we report on the developed and used of finite element methods, have been developed and used for sheet forming simulations since the 1970s, and have immensely contributed to ensure the success of concurrent design in the manufacturing process of sheets metal. During the forming operation, the Gurson–Tvergaard–Needleman (GTN) model was often employed to evaluate the ductile damage and fracture phenomena. GTN represents one of the most widely used ductile damage model. In this investigation, many experimental tests and finite element model computation are performed to predict the damage evolution in notched tensile specimen of sheet metal using the GTN model. The parameters in the GTN model are calibrated using an Artificial Neural Networks system and the results of the tensile test. In the experimental part, we used an optical measurement instruments in two phases: firstly during the tensile test, a digital image correlation method is applied to determinate the full-field displacements in the specimen surface. Secondly a profile projector is employed to evaluate the localization of deformation (formation of shear band) just before the specimen's fracture. In the validation parts of this investigation, the experimental results of hydroforming part and Erichsen test are compared with their numerical finite element model taking into account the GTN model. A good correlation was observed between the two approaches.

1. Introduction

Recently, virtual tools, such as numerical simulation using finite element methods (FEMs), is a useful tool to optimize the sheet metal forming process (hydro-forming, deep drawing, thermoforming, etc.) and to reduce the cost of final products. For the engineering community, an accurate estimation of the material parameters for constitutive models is often indispensable. The numerical simulation, taking into account damage in constitutive behavior of metallic materials, is necessary to develop a virtual model for various engineering problems involved in forming processes (necking, macroscopic cracks, fracture, etc.).

In recent decades, the attention of many researchers has been focused on understanding and modeling the basic mechanisms of ductile failure in metal forming process, Mediavilla et al. [1] developed a model to describe the complete evolution, from the initiation of damage to crack propagation during forming processes. Among many authors, Brünig and Ricci [2] and Badreddine et al. [3] proposed respectively an anisotropic and isotropic damage model to predict the instability phenomena appear in the different mechanical loading states during metal forming. Also the importance of the coupling between the damage and plasticity in numerical simulation has proved by Guo et al. [4]. In same context, Lin et al. [5] proposed an improvement in the Gurson model in order to will allow investigating in future other mechanical structures made up of ductile porous media. The pioneering work elaborated by Kachanov in 1958 [6], started the subject that is now known as Continuum Damage Mechanics (CDM).

From industrial point of view, the results obtained in this field are now very helpful in the preliminary design stage, particularly are widely used to avoid the failure during the forming process. Accordingly, many authors proposed constitutive equations of ductile damage. The most widely used approaches are based on the Gurson type modeling of ductile damage [7]. Inter alia, Tvergaard study the localization of deformation using Gurson model [8], the influence of voids on shear band instability [9] and the analysis of ductile failure by the voids evolution up to coalescence [10].

Experimental methods do not provide a complete stress analysis solution without additional processing of the data and/or assumptions about the structural system [11]. Also, it is obvious that in metal forming process, the results of numerical simulation depend strongly on the ability of the used constitutive equations to describe the physical phenomena accurately but the parameters values of the behavior law are also very important. For that, it is recommended to use a good technique in the evaluation of mate-

* Corresponding author. Tel.: +216 96 167 265; fax: +216 71 391 166.
E-mail address: fethi.abbassi@ipeib.rnu.tn (F. Abbassi).

http://dx.doi.org/10.1016/j.matdes.2012.09.032

Nomenclature

ANNGTN	Artificial Neural Networks model of GTN
TMSE	training mean square error
X	term of input
F_t	training function
P	pressure
H	dome height
E	Young's modulus (MPa)
v	Poisson's ratio
n	hardening coefficient
K	strength coefficient
$\bar{\varepsilon}$	equivalent true strain
ε_0	pre-strain
ϕ	plastic potential
f	void volume fraction
f_c	critical volume fraction
f_f	void volume fraction
f^*	modified void volume fraction
f_c	critical volume fraction
f_u^*	ultimate value of f^*
ε_{kk}^p	plastic hydrostatic strain
ε_n	mean effective plastic strain
S_n	standard deviation
f_n	nucleation micro-void volume fraction
(q_1, q_2, q_3)	fitting parameters
V_M	volume of the material without defects
V	volume of material
σ_m	hydrostatic stress (MPa)
σ_y	yield stress of matrix material (MPa)
$\overline{\sigma}$	von Mises equivalent stress (MPa)
$v(x, y)$ $u(x, y)$	homogenous displacement field for one pattern
a_1, b_1, a_2, b_2	elongation terms
a_3 and b_3	shearing terms

rial properties. Generally the parameter fits are processed by optimization methods. Exceptionally, the inverse methods offer a powerful tool for the identification of the parameters of the behavior law and the material properties of metals. The Principle of inverse identification method, that identifies a set of material parameters in a constitutive model, describes the complicated stress–strain responses by minimizing the difference between the test results and the results of the corresponding numerical simulation using an advanced optimization technique, but the inverse methods require prohibitive computing time because they usually use finite element computation coupled with an optimization procedure.

In order to resolve the problem of computing time in inverse identification process, this investigation presents a new ANNGTN Approach based on the Artificial Neural Network Method for the identification of GTN model parameters. A Design of Experience (DOE) method is used to select the suitable and the correct training base.

The remainder of this paper is structured as follows: the first paragraph will explain the principle of GTN ductile damage mainly the origin and the physical aspect that describe the micro-growth nucleation and mechanical effects of damage in ductile metals. The GTN model is also presented as it is one of the most widely employed models to evaluate the ductile damage and fracture. The second section gives an experimental investigation based on tensile test with notched specimen to determinate the evolution of the damage process in a ductile metal related to the macroscopic loading evolution using Digital Image Correlation (DIC). As used in this article, the term digital image correlation refers to the class of non-contacting methods that acquire images of an object, store images in digital form, and perform image analysis to extract full-field shape and deformation measurements in the specimen surface. After the fracture of specimen, the fracture topographies are analyzed by SEM in order to prove the use of GTN model. The third section is devoted to the identification programming procedure of ANNGTN model and the benefits of this technique in terms of computing time and reliable results. In the next section we will present two case studies: the hydroforming (bulge test) and the Erichsen test. Finally, conclusions are drawn in section five.

2. Modeling of ductile damage

2.1. Physical aspect of ductile damage

Damage phenomena of materials are generally investigated by means of a damage model, which can represent variations of material properties and processes of material failure due to damage initiation, growth, propagation and crack nucleation within the material [12]. Especially, in sheet metal forming industry, the localized necking failure is recognized as important limitation on metal formability. Two stages diffuse and local necking visually precedes the failure of ductile metals. The last one represents the result of damage evolution cited previously (Fig. 1). This phenomenon reacts inside material called ductile damage. During the analysis of the defect present in the forming process, especially the progress of failure in materials, many physical observation and micromechanical analysis have led to the development of a number of phenomenological or micro mechanical ductile fracture criteria [13,14] for the prediction of the rupture of metals in service. Principally, the damage criteria are classified into two approaches (i) uncoupled: which neglect the effects of damage on the yield surface of materials, and (ii) coupled: which incorporate damage accumulation into the constitutive equations.

2.2. GTN ductile damage model

The main purpose of the present work is to use ductile damage model to predict a sheet metal failure. In 1977, Gurson [15] developed a constitutive model to describe the micro-growth nucleation

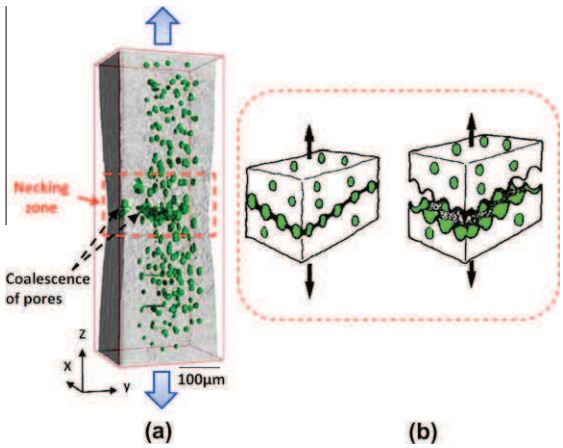

Fig. 1. Physical aspect of ductile damage (a): A reconstructed 3D image acquired during the loading process representing inner pore [13], (b): damage evolution in the necked region.

mechanical effects of damage in ductile metals, extended in 1984 by Tvergaard and Needleman [16] who incorporated some additional parameters (q_1, q_2, q_3). The yield function describing the plastic constitutive model is represented as follows:

$$\varphi(\sigma,\sigma_m,f)=\frac{\overline{\sigma^2}}{\sigma_y^2}+2f^*q_1\cosh\left(\frac{3}{2}q_2\frac{\sigma_m}{\sigma_y}\right)-(1+q_3(f^*)^2)=0 \qquad (1)$$

where q_1, q_2 and q_3 are a fitting parameters used to calibrate the model prediction of periodic arrays of spherical and cylindrical voids, with $q_3=(q_1)^2$, σ_m hydrostatic stress, σ_y yield stress of matrix material, $\overline{\sigma}$: von Mises equivalent stress, and f is the void volume fraction which is equal to $1-\frac{V_M}{V}$.

f^* represent the modified void volume fraction which is given as follows:

$$f^*=\begin{cases} f & \text{if } f\leqslant f_c \\ f_c+\frac{f_u^*-f_c}{f_f-f_c}(f-f_c) & \text{if } f>f_c \end{cases} \qquad (2)$$

where f_u^* represent the ultimate value of f^* which is defined as the stress carrying capacity vanishes, f_f represent the void volume fraction corresponding to failure, and f_c is the critical volume fraction where rapid coalescence occurs.

The instantaneous rate of growth of the void fraction depends both on nucleation of new voids and growth of pre-existing voids, it is given by:

$$df=\underbrace{(1-f)\cdot(d\varepsilon_{kk}^p)}_{growth}+\underbrace{ad\bar{\varepsilon}^p}_{nucleation} \qquad (3)$$

where ε_{kk}^p is the plastic hydrostatic strain and a defined as follows:

$$a=\frac{f_N}{S_N\cdot\sqrt{2\pi}}\cdot\exp\left[-\frac{1}{2}\cdot\left(\frac{\bar{\varepsilon}_p-\varepsilon_N}{S_N}\right)^2\right] \qquad (4)$$

where S_n the standard deviation, ε_n the mean effective plastic strain of nucleation and f_n the nucleation micro-void volume fraction represent.

3. Experimental setup

3.1. Full-field optical measuring methods

DIC is an application based on the comparison of two images acquired at different states during the deformation. Two subsets are chosen respectively from the reference and the next image used for the computation. The algorithm of correlation used to detect the local displacements of the pixels by comparing the two subsets, is as follows [17,18]. In practice, a single value is not a unique signature of a point, hence neighboring pixels are used. The matching of images taken by only one camera, at different time, on an object which becomes deformed is called temporal matching or tracking. From its principle, the correlation technique can be used correctly only with objects having a surface with a sufficiently random texture.

Two CCD (Coupled Charge Device) cameras were used to take digital images with a 1280 by 1024 pixels definition. These images are then analyzed by the Aramis software developed by the GOM

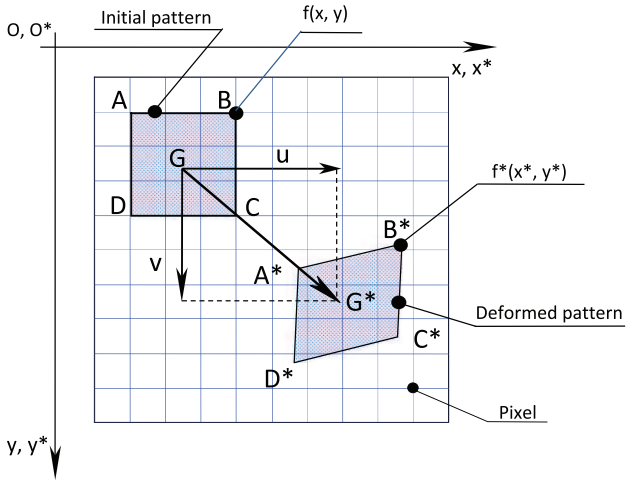

Fig. 2. Relative location of sub-images of the deformed and the undeformed patterns on the surface.

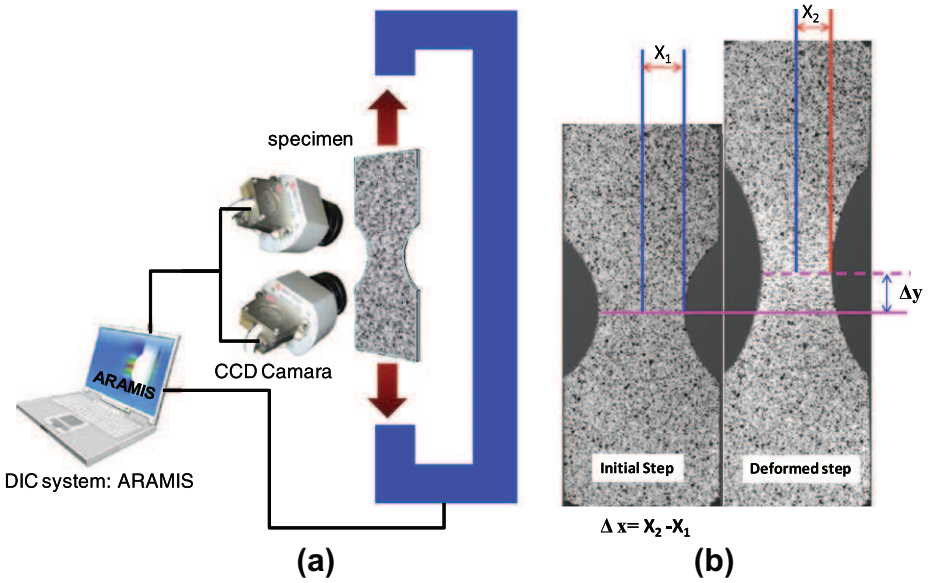

Fig. 3. (a) Experimental setup of uni-axial tensile test, (b) extracted results from tensile test with notched specimen.

society. This one gives a measure of the displacements and strain fields on the surface of an object within a precision of 200 μm/m. Aramis software is able to match correspondent points of an image by grey level analysis, if the surface of the specimen is covered with a black and white mapping, which forms a random grey-level. A gray level coded on 8 or 12 bits corresponds to each pixel of the CCD sensor. A succession of several pixels lying on the same line forms a grey level sequence. The fundamental principle lies in the fact that the distribution does not vary during the deformation of the object. It is therefore sufficient to follow this distribution of grey levels during their displacement to obtain the displacements of the corresponding point. This is made possible by the use of correlation domains which are $n \times n$ pixel gathering zones.

In the DIC method, the relation between the deformed image and the undeformed one is illustrated in Fig. 2. If we call G the central point of the subset in the initial configuration and $G*$ the corresponding central point of the subset in the deformed configuration, the relationship between the coordinates of these two points can be expressed by:

$$\begin{aligned} x^* &= x + u(x, y) \\ y^* &= y + v(x, y) \end{aligned} \tag{5}$$

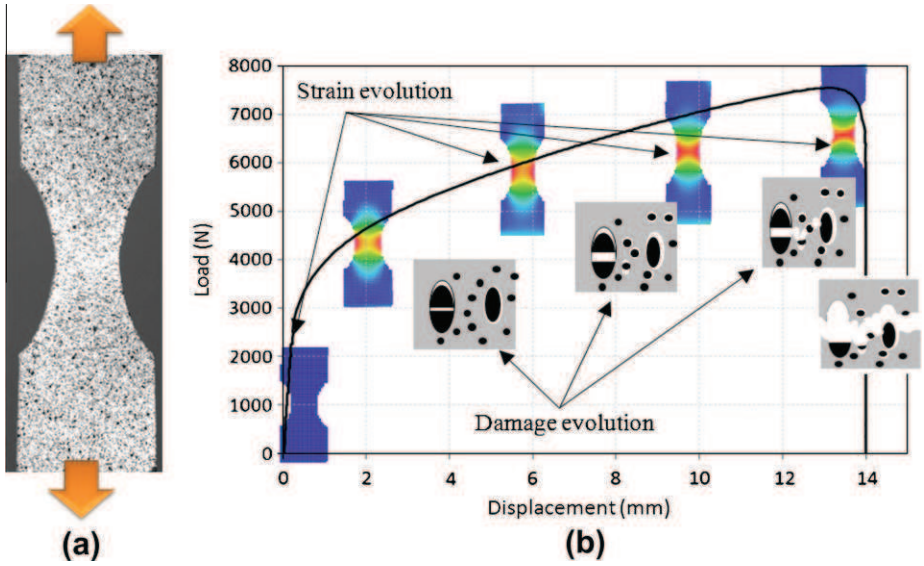

Fig. 4. (a) Tensile test of bi-entailed plate specimen, (b) evolution of the damage process in a ductile metal related to the macroscopic loading evolution.

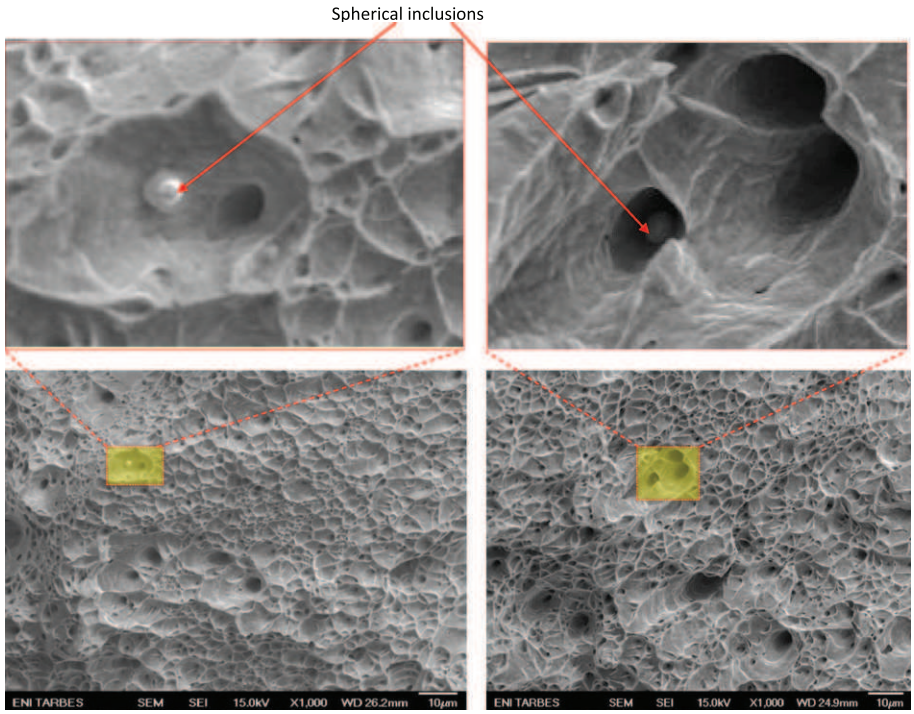

Fig. 5. Scanning electron microscope (SEM) views of fracture in tensile specimen (spherical inclusion observations).

where $u(x, y)$ and $v(x, y)$ represent the homogenous displacement field for one pattern (whole set of pixels).

In the Aramis software the displacement field is considered homogeneous and bilinear with respect to x and y:

$$\begin{cases} u(x,y) = a_1 \cdot x + a_2 \cdot y + a_3 \cdot x \cdot y + a_4 \\ v(x,y) = b_1 \cdot x + b_2 \cdot y + b_3 \cdot x \cdot y + b_4 \end{cases} \quad (6)$$

where a_4 and b_4 represent the terms of the rigid body motion, a_1, b_1, a_2 and b_2 represent the elongation terms and a_3 and b_3 are the shearing terms.

3.2. Tensile test with notched specimen

In the first part of the present investigation, a large experimental work has been done. Several low rate tensile tests were carried out in the laboratory on an INSTRON tensile test machine at a strain rate of 10^{-3} s^{-1}. In general, these studies involve the use of notched tensile specimens and measuring of the displacements and loads. The necked or notched regions contain large gradients of stress and strain which locates the voids growth. The notched specimens [19] were obtained using a laser cutting process from stainless steel sheet with uniform thickness 1 mm. A digital image correlation method was used to measure the displacement fields at the surface of the specimens during the tensile tests. Fig. 3 illustrates the specimen and the equipments used during this tensile test, the part (b) of this figure show the extracted parameters for use in the identification process (Δx, Δy). Fig. 4 shows the displacement-load curve, sequences of the progress of strain distribution until failure at different load levels obtained by Aramis software were we observed the localization of deformation and explain the voids growth up to fracture. The deformations in the specimen surface remains homogeneous until that the material damage becomes significant during the tension process, and the stress is a monotonic increasing function of the strain.

3.3. Fracture analysis by SEM observations

The onset of ductile fracture is initiated by void formation around non-metallic inclusions and second-phase particles in metal matrix that is subjected to plastic strain under the influence of external loading. Observations of the damage nucleation mechanisms have been carried out through in sit tensile tests at room temperature. Fig. 5 shows an example of SEM photograph of the fracture surface at failure. The spherical shape of the second phase particles and non-metallic inclusions present in the stainless steel can be considered the major reason for ductile fracture initiation. Several damage models were developed to describe this complex micro-mechanism in the sheet metal used in the forming process.

4. Artificial Neural Networks (ANN)

4.1. Artificial Neural Networks applications

The Artificial Neural Networks are today applied in many mechanical manufacturing processes [20,21]. Their ability to give effective results in the shortest time and their easy handling are very noticeable. The main objectives of ANN are to develop methods and models from experiment and examples for solving problems, usually solved by the conventional techniques such as the analytical algorithm and the programming software that enhance the intellectual activity of humans, for example: prediction, image recognition, classification, etc.

4.2. Artificial Neural Networks model of GTN damage (ANNGTN)

A better choice of neural network structure is a very important factor to ensure accurate results, the choice of function and learning algorithm, the choice of number of hidden layers and the neurons in each hidden layer are all factors that directly affect network performance [22].

For ANN model, we will use multilayer neural networks (MLNN) trained with a back-propagation supervised algorithm and composed by three layers: the input layer, the hidden layer and the output layer.

For a ANN composed by N neurons which the first layer noted C_1, $C_2 \ldots$, C_N and N weights noted $w_{(1)}$, $w_{(2)}$, $\ldots$, $w_{(N)}$, the term of input X can be determined by the following equation:

$$X = \sum w_{(i)} \cdot C_{(i)} + b \quad (7)$$

The back-propagation consists in optimization of the connection weights of the network which were initialized by going up layer by layer, of the output layer towards the input layer in order to minimize the TMSE (Training Mean Square Error) given by Eq. (8) calculated in the output S, see Eq. (9). The Training Means Square Error is given as:

$$\text{TMSE} = \frac{1}{2}\sum_{i=p}^{p}\sum_{k=1}^{k}(S_{ik} - o_{ik})^2 \quad (8)$$

where S_{ik} is the desired output (numerical value), O_{ik} the output of the current model, p represents the total number of layers and "k" is the output nodes number.

$$S = F_t \cdot X \quad (9)$$

X represents the input of a second layer that will be the balanced sum of the output values of the preceding neuron with a term of bias b (Eq. (7)).

$$F_t = \frac{1}{1 + e^{-X}} \quad (10)$$

The back-propagation algorithm used to adapt the neural network by comparing the result calculated on the basis of the inputs provided, and the response expected output. Thus, the network will change until it finds the right outputs [21,23].

The back propagation algorithm consists the following nine steps:

- *Step 1:* Choice of the training rate μ and the moment coefficient α
  - μ: Training rate, it is a constant ranging between 0 and 1 which fixes the training speed of the network.
  - α: Moment coefficient, generally takes a value ranging between 0.1 and 1; it makes it possible to accelerate the convergence of the algorithm.
- *Step 2:* Randomly initialization of the weights $w_{(i)}$.
- *Step 3:* Choice of the inputs sample and propagation of the calculation through the network.
- *Step 4:* Calculation of the outputs for all the neurons leaving the inputs layer towards the outputs layer.
- *Step 5:* Measure TMSE by difference between real output and desired output.
- *Step 6:* Algorithm stop: if calculated TMSE is lower than a threshold value of beforehand definite convergence, or if the iteration time is high.
- *Step 7:* Calculation of the contribution of one neuron to the error starting from the output and determination of the weight modification sign.
- *Step 8:* Correction of the neurons weights in order to decrease the error.

- *Step 9:* Repetition of calculation from step 3.

5. Identification of GTN parameters

5.1. Numerical modeling of notched tensile test

The proposed procedure of the damage law parameters require to develop a finite element model for the notched tensile test. Fig. 6a illustrates the geometric model of specimen developed according to the dimensions mentioned in mm [19]. Fig. 6b shows the meshed specimen with 3D hexahedral elements and the boundary conditions (BCs) of this model. This numerical simulation, takes into account the ductile damage of sheet metal by using GTN model.

5.2. Design of Experiment (DOE) methodology for ANNGTN

Classically, to develop a reliable ANN application, it is recommended to have a good training data selection. The design of experimental (DOE) methodology used in many research works. Particularly, Ledoux et al. [24] used this technique in the optimization of parameters forming process. In this investigation, the design of experimental method allows the study of sensibility of the numerical response according to GTN parameter's variation. In this identification process of ductile damage parameters, we use a factorial design in order to decrease the number of numerical simulations. For each variable, two levels are used, the low and the high parameter value to represent the limits of variations (Table 1). The material parameter's constitutive of GTN model are $\{f_f, f_0, f_N, \varepsilon_N, S_N\}$.

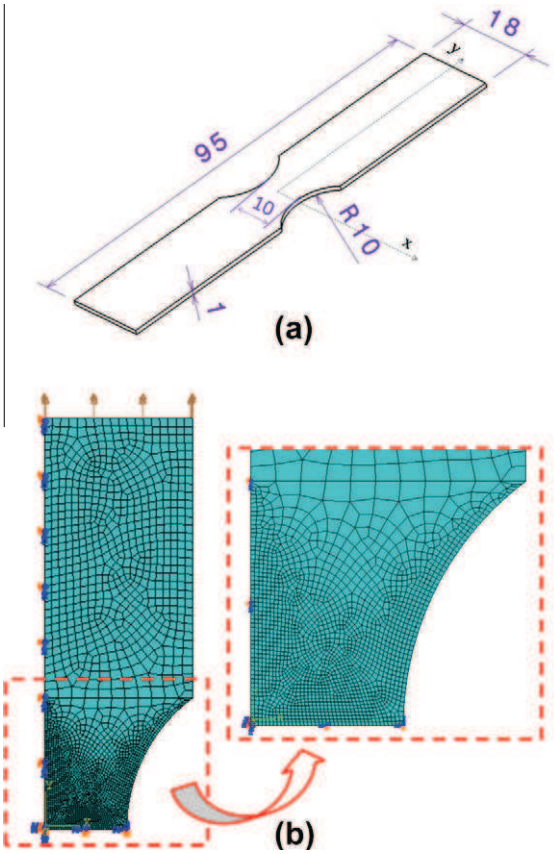

Fig. 6. (a) Geometry and dimensions (mm) for the notched tensile test, (b) numerical model of tensile test with notched specimen.

Table 1
ANNGTN training base developed using DOE methodology.

Experiment number	OUTPUT data					INPUT data
	Factor: (parameter's of GTN model)					
	f_f	f_c	ε_n	S_n	f_n	
1	0.118	0.11	0.66	0.11	0.044	The point of the *X* and *Y*
2	0.118	0.11	0.66	0.11	0.036	displacements curve of
3	0.118	0.11	0.66	0.09	0.044	the specimen middle
4	0.118	0.11	0.66	0.09	0.036	point (results of
5	0.118	0.11	0.54	0.11	0.044	numerical simulation
6	0.118	0.11	0.54	0.11	0.036	using Abaqus software)
7	0.118	0.11	0.54	0.09	0.044	
8	0.118	0.11	0.54	0.09	0.036	
9	0.118	0.09	0.66	0.11	0.044	
10	0.118	0.09	0.66	0.11	0.036	
11	0.118	0.09	0.66	0.09	0.044	
12	0.132	0.11	0.66	0.11	0.044	
13	0.132	0.11	0.66	0.11	0.036	
14	0.132	0.11	0.66	0.09	0.044	
15	0.132	0.11	0.66	0.09	0.036	
16	0.132	0.11	0.54	0.11	0.044	
17	0.132	0.11	0.54	0.11	0.036	
18	0.132	0.11	0.54	0.09	0.044	
19	0.132	0.11	0.54	0.09	0.036	
20	0.132	0.09	0.66	0.11	0.044	
21	0.132	0.09	0.66	0.11	0.036	
22	0.132	0.09	0.66	0.09	0.044	

5.3. ANNGTN identification strategy and results

In the work published by Abbassi et al. [25,26], an inverse identification method was developed for the determination of the hardening low parameter's using bulge test. In this identification process, first a coarse research is carried out by the Monte Carlo Algorithm which was refined in second step by Levenberg–Marquardt Algorithm. The extracted results were used in this identification procedure of the damage parameters.

For the reason of the diversity of the method proposed in literature for identification of the GTN model parameters, Benseddiq and Imad [28] develop a global analysis of the data which gives numerous values of GTN parameters from the literature, a large variability of this parameter for a considered material was observed. According to this analysis [28] we can subdivide the parameters in two principal's families:

(i) Constitutive parameters (q_1, q_2, and q_3). The constitutive parameter q_1 varies from 1.1 to 1.5 for many materials. However, this parameter is often fixed q_1 to 1.5 and q_2 to 1.
(ii) Material parameters. This family also can be classified in two parts: the first part cover the initial material f_0, and nucleation parameters f_n, S_n and ε_n, the value $\varepsilon_n = 0.3$ and $S_n = 0.1$ have been used in several studies. The second part describes the critical and final failure parameters (f_c, and f_f). Tvergaard and Needleman [27] recommended that the value of f_c can be taken as 0.15. The final failure void volume fraction f_f is considered a parameter that may be experimentally determined [28]. Originally, Tvergaard and Needleman [27] proposed a value $f_f = 0.25$.

Our Artificial Neural Networks model is developed under MatLab software. Firstly, the identification procedure of GTN ductile damage parameters started by the training of ANN using the results ($\Delta x, \Delta y$) of many simulation of notched tensile test carried out under ABAQUS software. The different combinations of the input parameters of ductile damage model are based on the experimental design presented in the previous section. Secondly, in the generalization step, we introduced the experimental data obtained

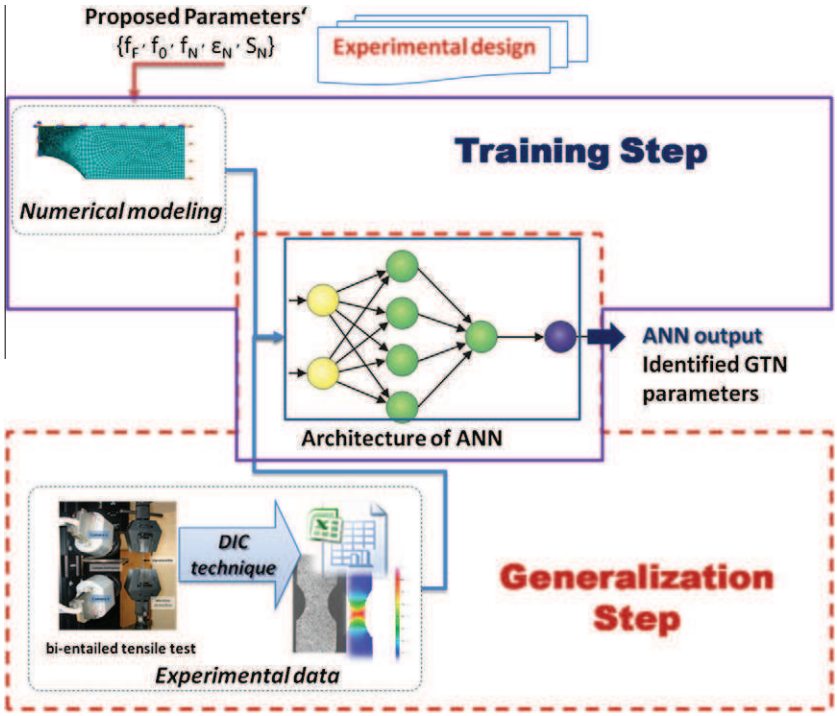

Fig. 7. Damage parameters identification procedure using ANN and experimental data.

by using the digital image correlation in the notched tensile test in order to identify the damage low parameters. Fig. 7 summarizes the identification procedure and the ANN model structure. In the input layer's, there are two neurons that represent the elongation of the specimen in the two directions (Δx, Δy). In the hidden layer, we found 10 neurons. Finally in the output layer it has five neurons and each one represent the GTN parameters.

It is recommended to choose an optimal structure of ANN in order to obtain reliable results in the identification procedure. The multi-layer neural network with three layers is the most frequently used structure in ANN model. Generally used with a sigmoid transfer function and a gradient descent method of training called the back-propagation training algorithm (Table 2). The difference between the used structures principally appears in the number of neurons in each layer, because this last one has a direct relation with the number of parameters in the input and output layer. For the hidden layer no specific formula fixed for the choice of number of neurons, but it directly influenced by the nature of the input data. For that it is difficult to have a uniform structure. To provide the optimal structure of our ANN (Table 2), we started by setting the inputs and outputs, training algorithm, the number of hidden layers and the number of neurons in each hidden layer, etc.

In order to validate the results obtained by our ANNGTN model developed under Matlab, we prepared many test cases and compared the obtained results with the results of the finite element models. The comparison was presented in Fig. 8, for five testing cases. The result obtained by the ANN approach is in good agreement with the results obtained by the finite element model.

We consider the experimental data (Δx, Δy) as an input of the ANNGTN model to obtain the Gurson model parameters in output.

Table 2
Example of used structure for the ANN.

	ANNGTN	Abendroth et al. [29]	Marouani et al. [30]
Neurons in the input layer	2	6	10
Number of hidden layers	1	1	1
Neurons in the hidden layer	10	50	14
Neurons in the output layer	5	1	5
Training algorithm	Back-propagation	Back-propagation	Back-propagation
Activation function	Sigmoïd	Sigmoïd	Sigmoïd
Training coefficient	0.001	–	–

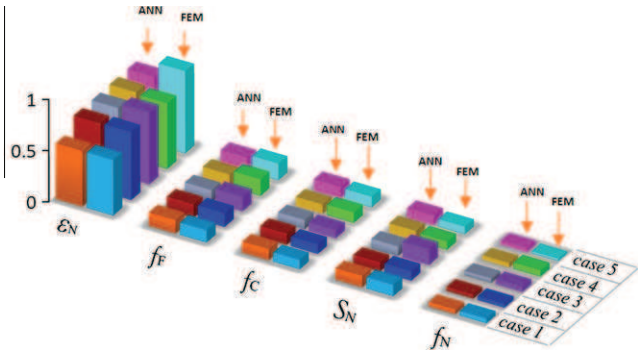

Fig. 8. Comparison between prediction using ANN and the results of FEM of different GTN coefficients.

Table 3
GTN identified parameters using ANN.

Parameters	Element number
Void volume fraction for coalescence (f_c)	0.11
Void volume fraction for element deletion (f_f)	0.118
Volume fraction of nucleating particules (f_n)	0.044
Mean nucleation strain (ε_n)	0.57
Standard deviation of nucleation strain (S_n)	0.09

Table 3 presents the identification results of the damage parameters of the stainless steel 304. Using SEM image analysis, Chhibber et al. [31] demonstrated that for the SS304 the final volume fraction f_f is less compared with the others steels, whereas the percentage change in void volume fraction values from initial void volume fraction to final void volume fraction it' is height. This corroborates with the very high ductility of SS 304 austenitic stainless steel often used in metal forming. The big advantage of this method is to minimize the computing time in the classical inverse identification process of the GTN model parameters.

5.4. Comparison between numerical and experimental results in tensile test

During the experimental tensile test of the notched specimen the loading of specimen was stopped immediately after the observation of strain localization. In the second step, the middle centre of specimen was digitalised in order to show the appearance of the shearing band using high precision optical profile projector, Fig. 9b shows the results of the scanning. A huge reduction of thickness in the local zone of the specimen (57 μm) was observed. Also in Fig. 9a, the results of numerical simulation of this test are present. Qualitatively, a same mechanism of necking initiation is presented in numerical and experimental results. This observation demonstrate the ability of finite element modelling taking into account the ductile damage of material to predict the physical phenomenon faithfully.

6. Applications

6.1. Elliptical bulge test

In order to evaluate the results of GTN identification, several experimental bulge tests were developed. During this test, a circular blank is clamped at its external boundary between a die and blank holder by a drawbeads and a linearly increasing hydraulic pressure is applied on the bottom surface of the blank. The displacement of the dome is measured continuously. An elliptical die was used, the dimensions of major and minor axis was respectively 110 mm and 74 mm. The sheet with a uniform thickness 1 mm is meshed using thin shell elements with reduced integration of type S4R and the matrix is considered as rigid body meshed with rigid elements of type R3D4. The identified damage parameters were used in the simulation of the elliptical bulge test and the experimental and numerical results were compared. Fig. 10a and b respectively show the numerical failure prediction and the exper-

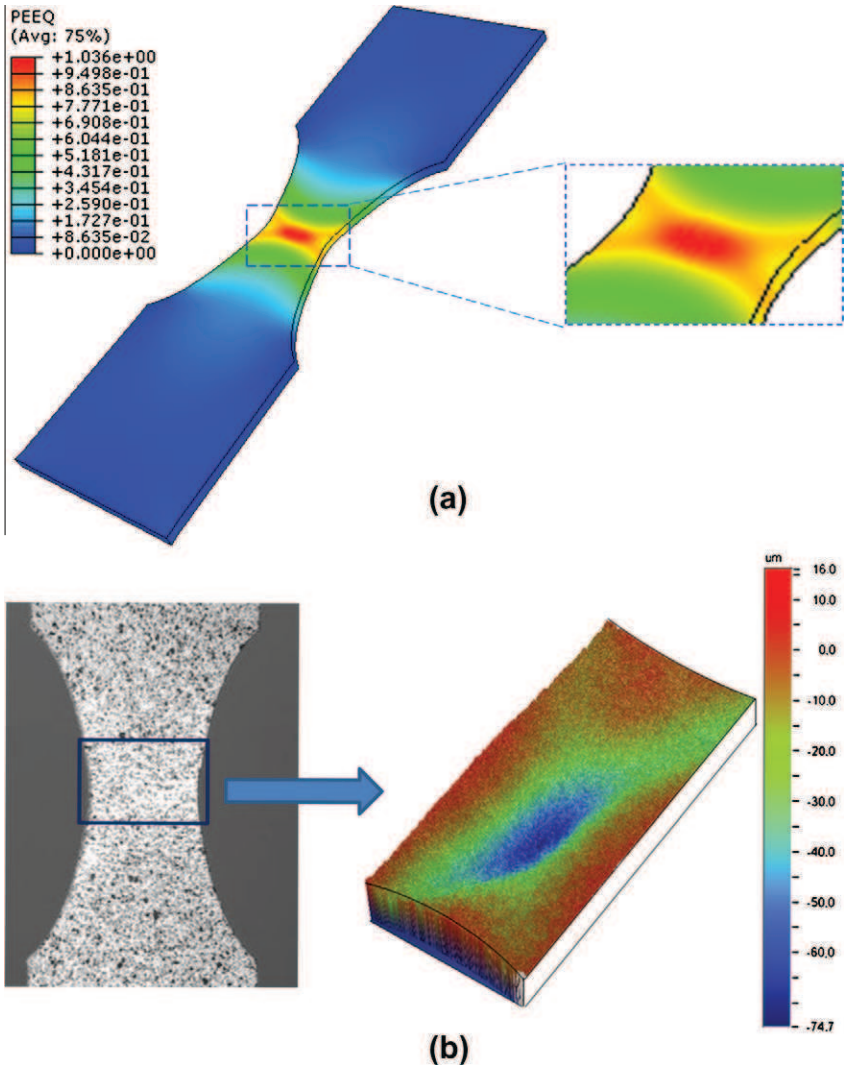

Fig. 9. Localisation of deformation: (a) numerical prediction of band formation using GTN model, (b) experimental digitalisation of middle centre of specimen just before fracture.

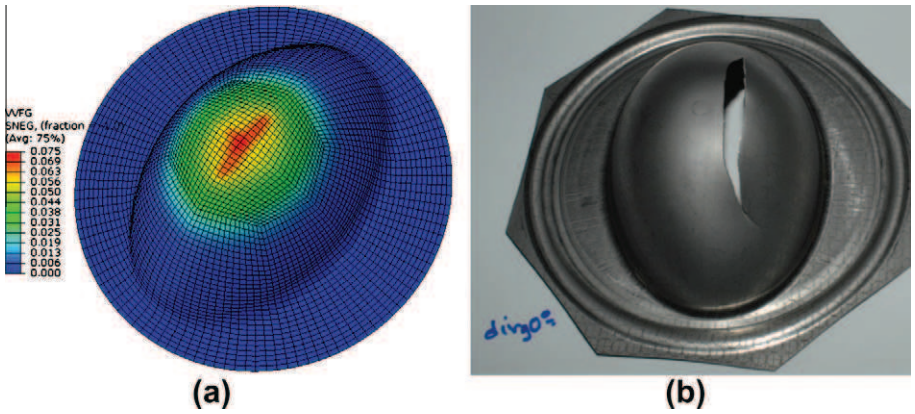

Fig. 10. (a) Numerical prediction of void volume fraction, (b) experimental specimen after cracking for elliptical bulge test.

imental fracture. A good qualitatively correlation between the numerical and experimental results is observed. Also Fig. 11 shows the numerical and the experimental curves evolution of dome position during the bulge test according to the pressure load. The

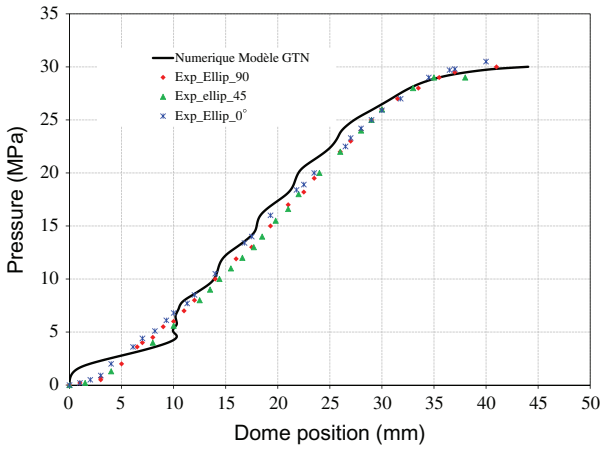

Fig. 11. Numerical and experimental comparison of dome position evolution according to the pressure load.

experimental curves Exp_Ellip_90, Exp_Ellip_45 and Exp_Ellip_0 respectively represent the evolution of dome position according to the internal pressure of the elliptical bulge test with the major axes of die oriented 90°, 45° and 0° with the rolling direction of the sheet. A small difference between the two results is observed, which is mainly due to the GTN model having isotropic nature.

The thickness variation is used as an indicator of the risks undergone in the part at the forming process. For these reasons, it is recommended to evaluate the thickness variation during the development of a manufacturing process. Gutscher [32] founds that the behaviour law parameters has significant influence on the height and thickness in the bulge test. In this context, the fringe pattern projection was used in this investigation to measure the deformed shape thickness. The basic principle behind the approach is to project known patterns on the deformed part using a digital projector. Two digital cameras are used to take images of the object with the known projection patterns imposed on it. Usually multiple projection patterns are used in a single measurement step to enhance accuracy. The results of this measurement technique were compared with the numerical results obtained by the FE model of bulge test based of the ductile damage. Fig. 12 shows that the results of numerical simulation and experiment agree well. Overall, despite all nonlinearities arising from the elasto-plastic behaviour of the sheet metal, the comparison of the numerical results with

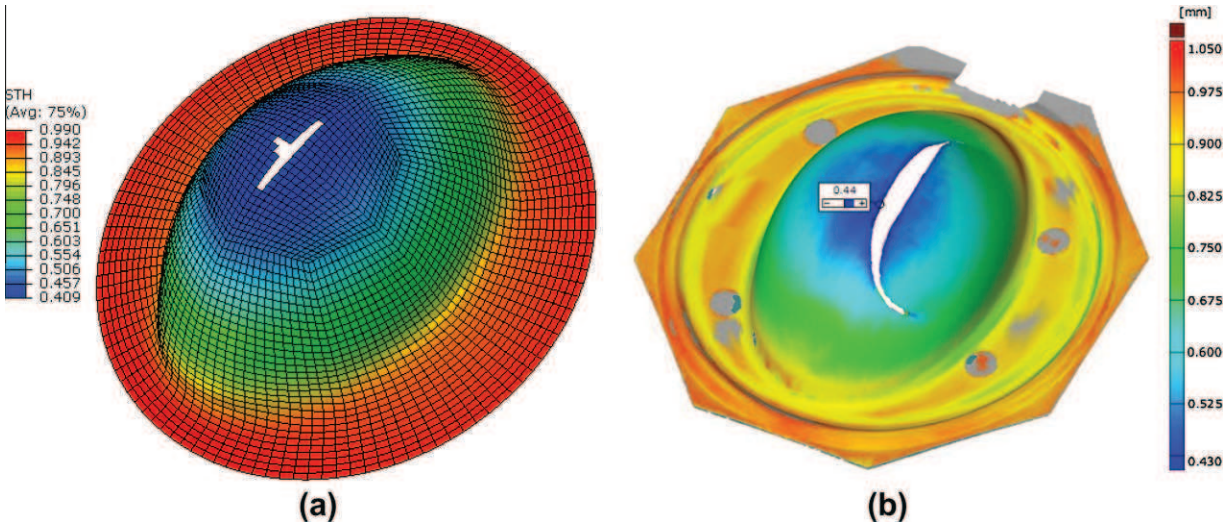

Fig. 12. Thickness variation in deformed parts, (a) numerical results, (b) experimental results.

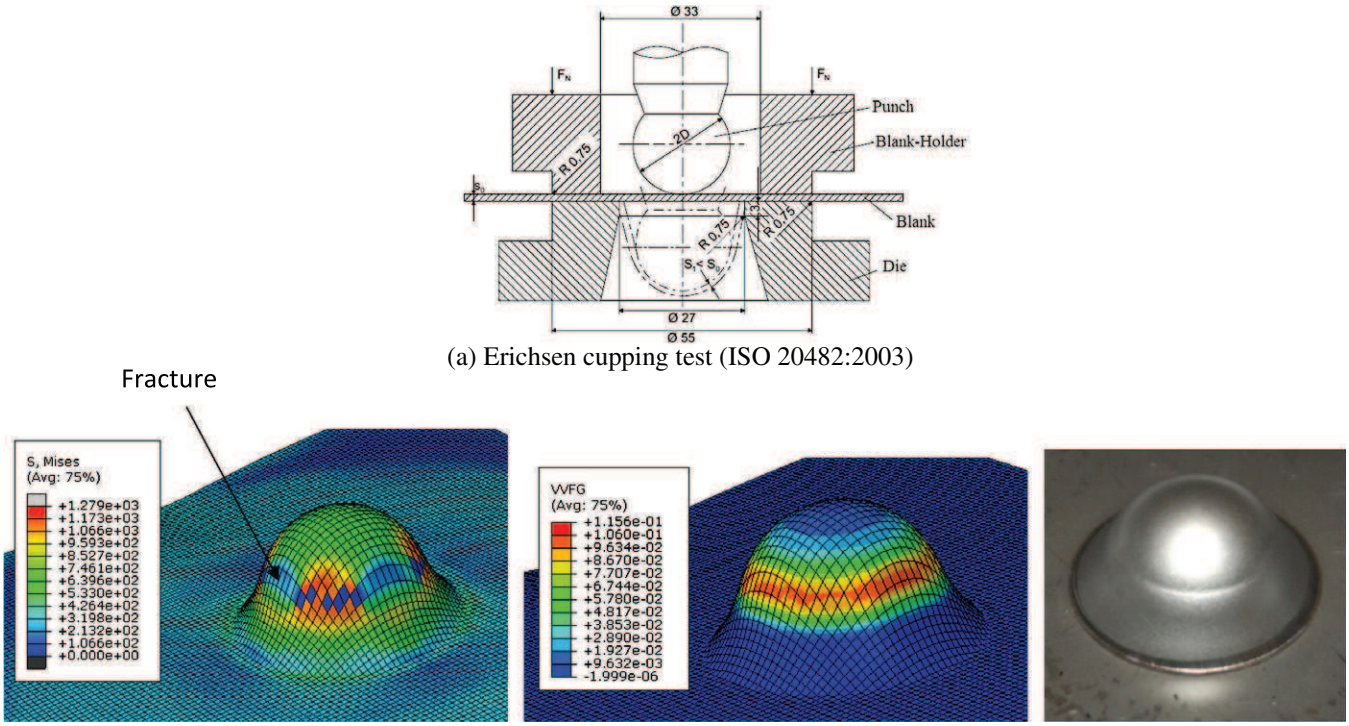

(a) Erichsen cupping test (ISO 20482:2003)

(b) Numerical von Mises Stress (c) void volume fraction due to growth (d) Experimental fracture

Fig. 13. Erichsen test experimental and numerical results.

the experimental results of elliptical bulge test shows the robustness of the numerical model.

6.2. Erichsen test

The geometry of the tools of Erichsen test (ISO 20482) [33] is defined by a hemispherical punch of steel with the diameter of 20 mm, an active die with the diameter of 27 mm, a blank holder with the diameter of 33 mm and a initial blank with a square shape 90 × 90 mm (Fig. 13a). The edge radius of die is 0.75 mm. The principle of Erichsen test means to press the hemispherical punch into the sheet until material fracture occurs, at which point the test is stopped immediately and the depth of the bulge recorded. This depth expressed in millimetres gives the Erichsen index (I_E), in our case, the experimental I_E of stainless steel 304 is 13.02 mm (Fig. 13d).

The finite element simulation model of Erichsen test consists of forming rigid bodies which are punch, die, and blank holder in addition to the blank as a deformable body. We used an elasto-plastic constitutive law taking into account the damage mechanics based on GTN model with the identified parameters. Fig. 13b and c shows respectively the von Mises stress distribution in deformed shape and the map of void volume fraction in the deformed shape. We observe a circumferential rupture of the specimen appear in same area in the experimental test and the numerical prediction. In the numerical model the Erichsen index, I_E = 12.83 mm. The small differences may be caused by the numerical modeling of the contact phenomena and the anisotropy of sheet.

7. Conclusions

In the present investigation, the Gurson–Tvergaard–Needleman (GTN) model was employed to evaluate the ductile damage and fracture phenomena. An identification procedure based on Artificial Neural Network is used to determine the material parameters of GTN damage model. A back propagation training neural network model was trained by using the finite element results of notched tensile test with varying of the damage parameters. A better choice of ANN structure and the concordance of the inputs allow to make more efficient ANN model.

The optical metrology and especially the DIC method are rapidly gaining popularity in light of the wealth of available results and the availability of commercial hardware and software. Through these means of measurement we obtain the displacements in all points on specimen surface and we compare closely the experimental results of shear band formation and the thickness variation in bulged part with the numerical results. The Identified parameters used in the Finite element model of forming operation (tensile, bulge and Erichsen tests), these results were in good agreement with experimental ones. Following this comparison we can summarize that our approach will be able to give a reliable results and good efficiency for the identification of damage parameters.

The proposed approach based on finite element coupled with ANN can be used in order to contribute towards the sheet metal characterization, but with a minimized computing time (CPU time) compared with the classical inverse identification method. On the other hand extension of this approach to the Gurson damage model coupled with anisotropic yield criterion will be also investigated.

References

[1] Mediavilla J, Peerlingsb RHJ, Geers MGD. An integrated continuous–discontinuous approach towards damage engineering in sheet metal forming processes. Eng Fract Mech 2006;73(7):895–916.
[2] Brünig M, Ricci S. Nonlocal continuum theory of anisotropically damaged metals. Int J Plast 2005;21(7):1346–82.
[3] Badreddine H, Saanouni K, Dogui A. On non-associative anisotropic finite plasticity fully coupled with isotropic ductile damage for metal forming. Int J Plast 2010;26:1541–75.
[4] Guo YQ, Li YM, Bogard F, Debray K. An efficient pseudo-inverse approach for damage modeling in the sheet forming process. J Mater Process Technol 2004;151:88–97.

[5] Lin J, Kanit T, Monchiet V, Shao J-F, Kondo D. Numerical implementation of a recent improved Gurson-type model and application to ductile fracture. Comput Mater Sci 2010;47:901–6.
[6] Voyiadjis George Z, Kattan Peter I. Advance in damage mechanics. Elsevier; 2006.
[7] Gelin JC, Oudin J, Ravalard Y. An improved FEM for the analysis of the damage and ductile fracture in cold metal forming processes. Ann. CIRP 1985;34(1):209–13.
[8] Tvergaard V. On localization in ductile materials containing spherical voids. Int J Fract 1982;18:237–52.
[9] Tvergaard V. Influence of voids on shear band instabilities under plane strain conditions. Int J Fract 1981;17:389–407.
[10] Tvergaard V. Material failure by void growth to coalescence. Adv Appl Mech 1990;27:83–151.
[11] Sharpe Jr William N. Springer handbook of experimental solid mechanics. Springer; 2008.
[12] Zhang Wohua, Cai Yuanqiang. Continuum damage mechanics and numerical applications. Zhejiang University Press, Springer; 2010.
[13] Mammoli AA, Brebbia CA. Characterization III. vol. 57. Transactions of the Wessex Institute; 2007.
[14] Brunet M, Morestin F, Walter H. Numerical analysis of failure in sheet metal forming with experimental validation. Revue Européennes des Eléments Finis 2-3-4; 2001, p. 275–93.
[15] Gurson AL. Continuum theory of ductile rupture by void nucleation and growth. I. Yield criteria and flow rules for porous ductile media. J Eng Mater Technol 1977;99:2–15.
[16] Tvergaard V, Needleman A. Analysis of the cup-cone fracture in a round tensile bar. Acta Metall 1984;32(1):157–69.
[17] Sutton MichaelA, Orteu Jean-José, Schreier Hubert W. Image correlation for shape, motion and deformation measurements: basic concepts, theory and applications. New York (USA): Springer; 2009.
[18] Sutton MA, Wolters WJ, Peters WH, Ranson WF, McNeill SR. Determination of displacements using an improved digital correlation method. Image Vision Comput 1983;1(3):133–9.
[19] Picart P, Ghouati O, Gelin JC. Optimization of metal forming process parameters with damage minimization. J Mater Process Technol 1998;80–81:597–601.
[20] Chamekh A, BelHadjSalah H, Hambli R, Gahbiche A. Inverse identification using the bulge test and artificial neural networks. J Mater Process Technol 2006;177:307–10.
[21] Sivasankaran S, Narayanasamy R, Jeyapaul R, Loganathan C. Modelling of wrinkling in deep drawing of different grades of annealed commercially pure aluminium sheets when drawn through a conical die using artificial neural network. Mater Des 2009;30:3193–205.
[22] Singh SK, Gupta AK. Application of support vector regression in predicting thickness strains in hydro-mechanical deep drawing and comparison with ANN and FEM. CIRP J Manuf Sci Technol 2010;3:66–72.
[23] Kim Hong-Gyoo, Sim Jae-Hyung, Kweon Hyeog-Jun. Performance evaluation of chip breaker utilizing neural network. J Mater Process Technol 2009;209:647–56.
[24] Ledoux Y, Samper S, Favrelière H, Formosa F, Pairel E. Optimisation of a stamping process by a design of experiments linked to a modal analysis of geometric defects. Arch Civil Mech Eng 2006;VI(1).
[25] Abbassi F, Pantalé O, Dalverny O, Zghal A, Rakotomalala R. Parametric sheet metal characterization by using Monte-Carlo and Levenberg–Marquardt: bulge test application. In: APCOM'07 in conjunction with EPMESC XI, December 3–6, Kyoto, Japan; 2007.
[26] Abbassi F, Pantalé O, Mistou S, Zghal A, Rakotomalala R. Effect of ductile damage evolution in sheet metal forming: experimental and numerical investigations. Key Eng Mater 2010;446:157–69.
[27] Tvergaard V, Needleman A. Analysis of the cup-cone fracture in around tensile bar. Acta Metall 1984;32:157–69.
[28] Benseddiq N, Imad A. A ductile fracture analysis using a local damage model. Int J Press Vess Pip 2008;85(4):219–27.
[29] Abendroth M, Kuna M. Identification of ductile damage and fracture parameters from the small punch test using neural networks. Eng Fract Mech 2006;73:710–25.
[30] Marouani H, Aguir H. Identification of material parameters of the Gurson–Tvergaard–Needleman damage law by combined experimental, numerical sheet metal blanking techniques and artificial neural networks approach. Int J Mater Form 2012;5(2):147–55.
[31] Chhibber R, Arora N, Gupta SR, Dutta BK. Estimation of Gurson material parameters in bimetallic weldments for the nuclear reactor heat transport piping system. Proc Inst Mech Eng, Part C J Mech Eng Sci 2008;222:2331.
[32] Gutscher G, Wu HC, Ngaile G, Altan T. Determination of flow stress for sheet metal forming using the viscous pressure bulge (VPB) test. J Mater Process Technol 2004;146(1):1–7.
[33] ISO 20482. Metallic materials – sheet and strip – Erichsen cupping test. Geneva: International Organization for Standardization (ISO); 2003.